Supplement of The Cryosphere, 16, 4679–4700, 2022
https://doi.org/10.5194/tc-16-4679-2022-supplement

The Cryosphere Open Access EGU

Supplement of

The contribution of Humboldt Glacier, northern Greenland, to sea-level rise through 2100 constrained by recent observations of speedup and retreat

Trevor R. Hillebrand et al.

Correspondence to: Trevor R. Hillebrand (trhille@lanl.gov)

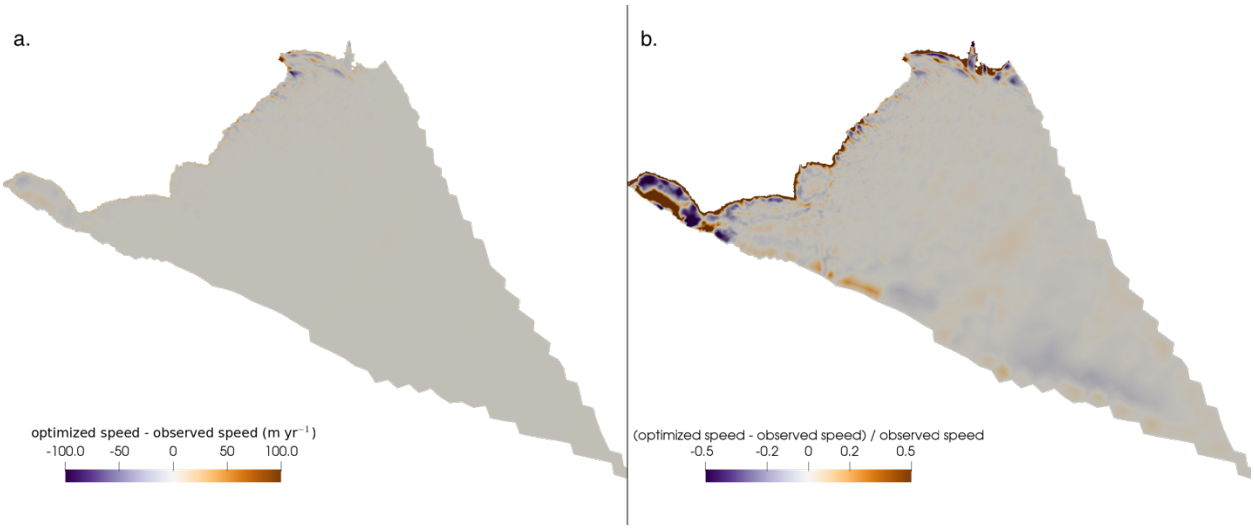

Figure S1: Absolute (a) and relative (b) error between optimized and observed velocities for the initial condition at 2007.

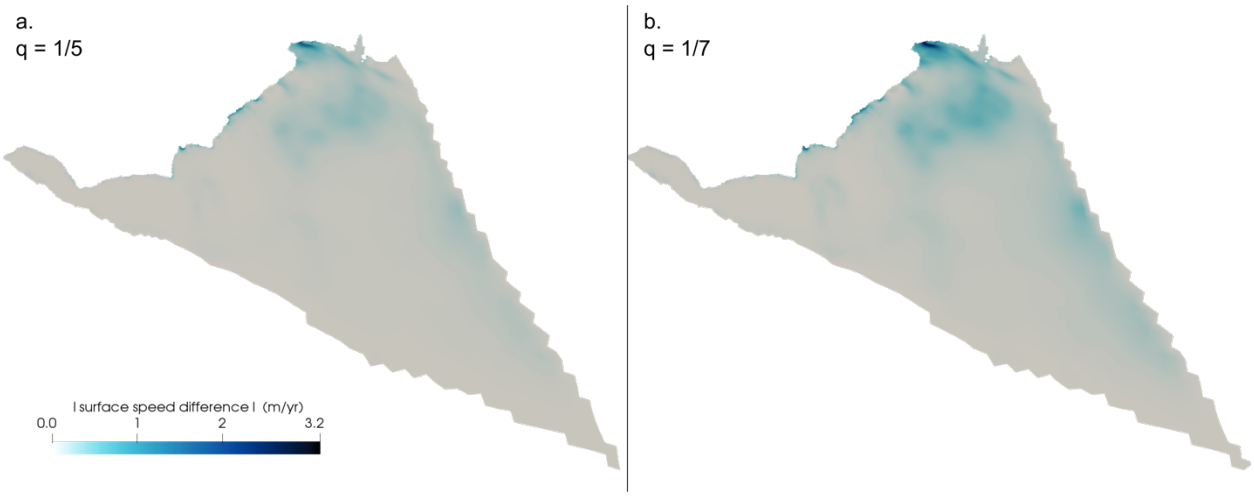

Figure S2: Absolute value of velocity difference using recalculated friction parameter μ for $q = 1/5$ (a) and $q = 1/7$ (b) relative to the optimization using $q = 1/3$ for a velocity solution at the initial condition in 2007.

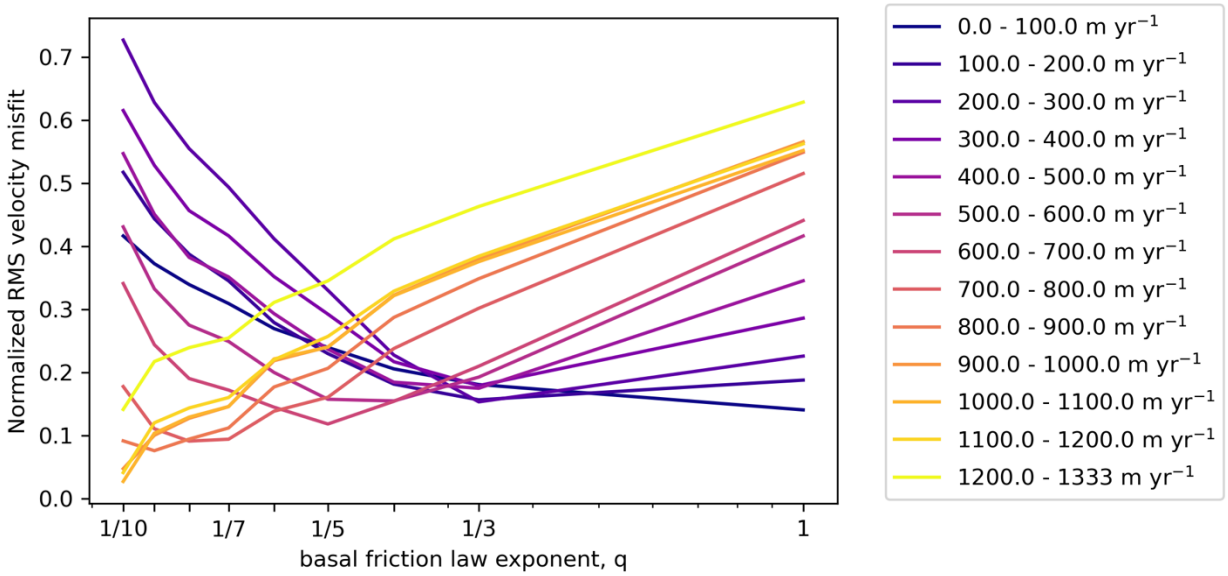

Figure S3: Results of the basal friction law exponent calibration step, using many more velocity bands than shown in Figure 3 of the main text.

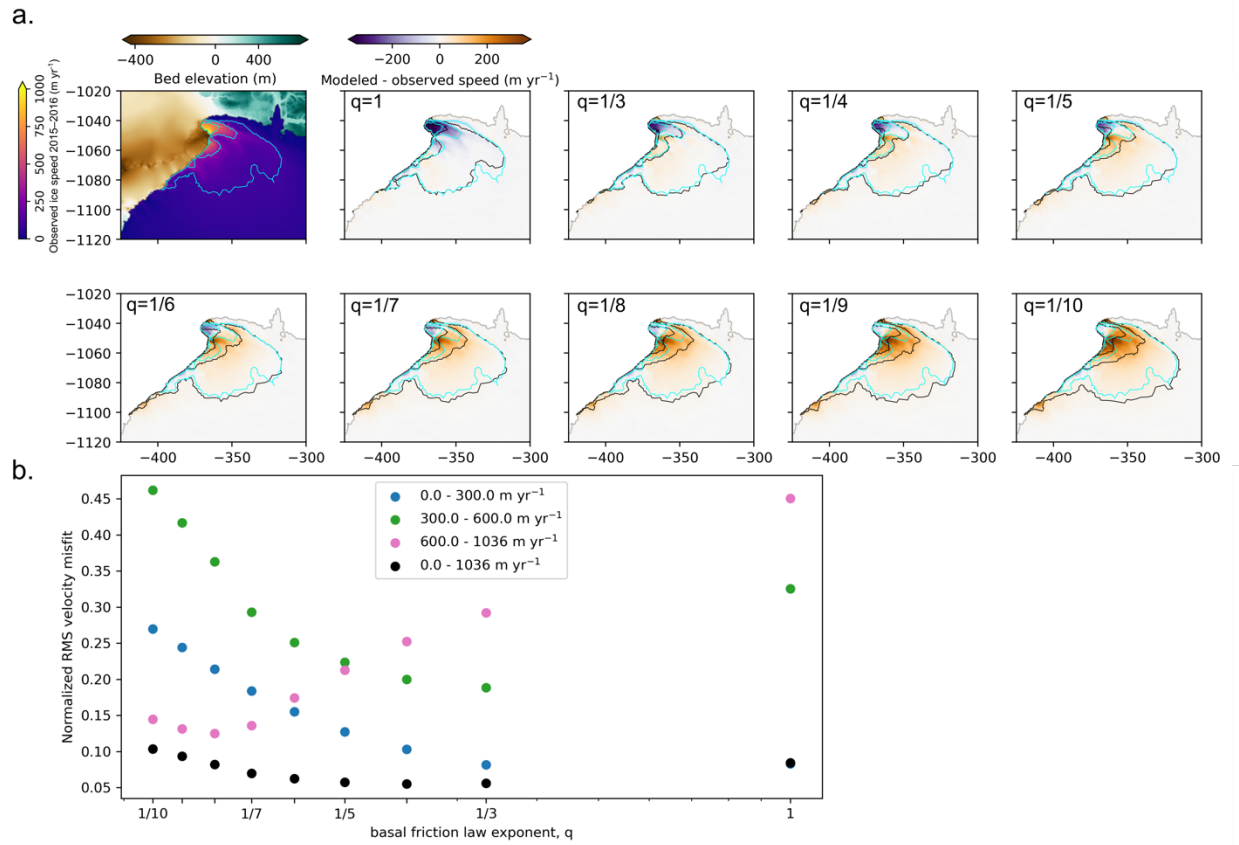

Figure S4: Same as Figure 3 in the main text, except with simulations using imposed retreat to the 2015–2016 margin instead of the 2017–2018 margin.

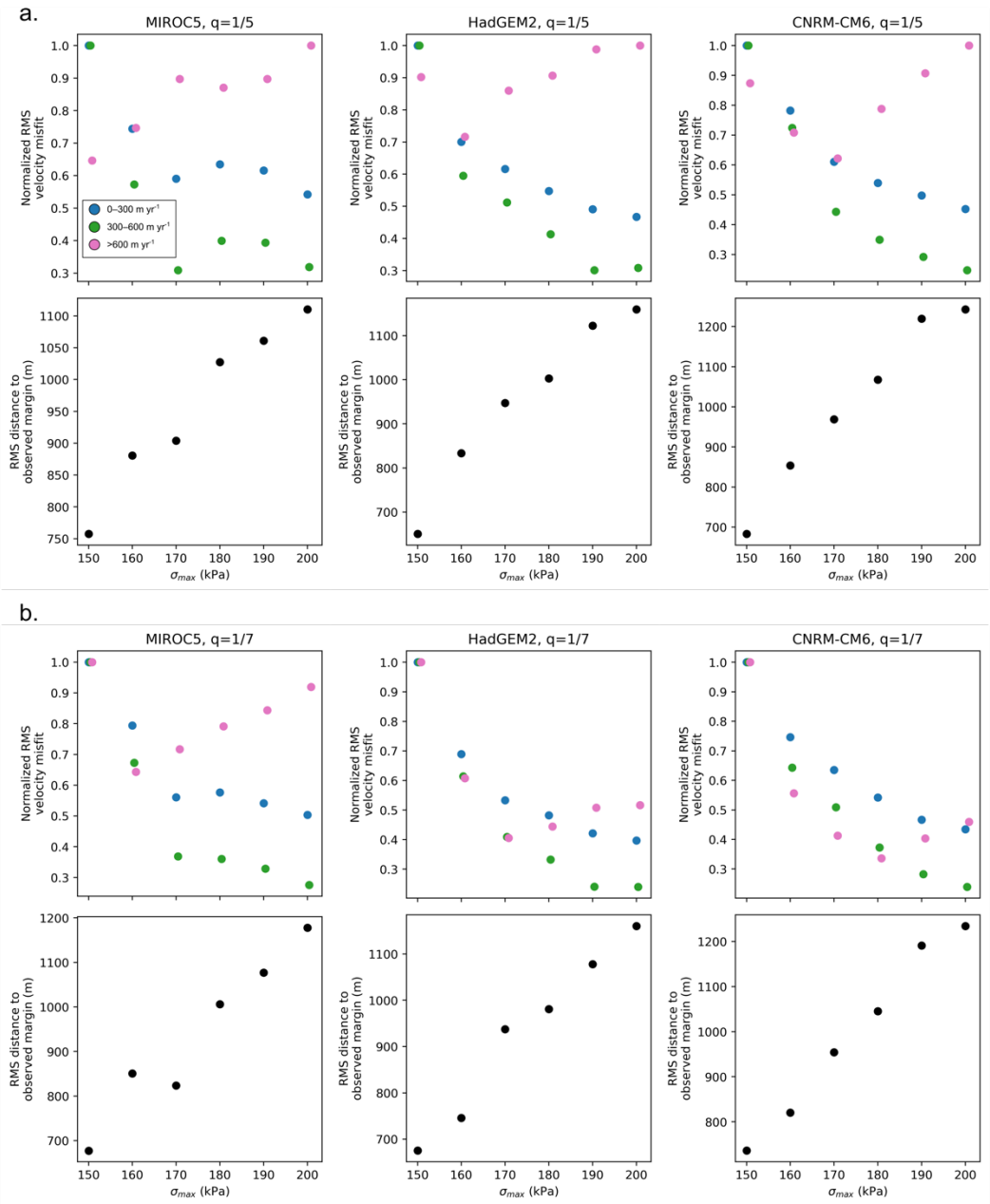

Figure S5: Results of tuning runs for von Mises stress calving law for q=⅕ (a) and q=1/7 (b). RMS velocity misfits are normalized by the maximum misfit in each velocity band, for ease of visualization. Modeled velocities and margin positions are compared with observations from 2017–2018 (Joughin et al., 2018). Values of σ_{max} chosen for century-scale projections are listed in Table 1. Slight horizontal offsetting of colored dots is to ensure visibility when multiple velocity bands have the same normalized RMS misfit value.

Mesh convergence

Previous work with MALI has shown accurate simulation of grounding-line dynamics at 1 km resolution (Hoffman et al., 2018, 2019). However, these studies included buttressing ice shelves and did not use a pressure-dependent power-law basal friction relationship. We performed a set of four simulations to determine the influence of mesh resolution on the modeled behavior of Humboldt Glacier using variable-resolution meshes with cell spacing of 0.25 – 10 km, 0.5 – 10 km, 1 – 10km, and 3 – 30km. We applied a Gaussian filter with a radius of 3 km to the BedMachine v4 bed topography and ice thickness datasets before interpolating to the meshes for these experiments,

to ensure that model behavior is controlled by model physics and not simply by resolving features of the bed topography. All simulations were run from 2007–2050 using surface mass balance and ocean thermal forcings from the MIROC5 RCP8.5 scenario. For the mesh convergence tests, submarine melt beneath ice shelves and at grounded margins are implemented as described above, calving is not applied, and we use a basal friction law exponent of q=1/5.

We find that our 1–10 km resolution mesh agrees well with results from the 0.25–10 km and 0.50–10 km meshes, while the 3–30 km mesh gives considerably different results in terms of changes in volume above floatation and grounded ice area (Figure S5). Thus, we choose the 1–10 km mesh for all simulations in the perturbed parameter ensemble as the best trade-off between accuracy and computing cost. We note that simulations using the von Mises stress calving law do not converge monotonically with increasing resolution, likely because of large stress gradients near the glacier terminus; the calving law would likely have to be tuned independently for each resolution, making the results of a convergence test ambiguous. This convergence test does not examine the dependence of the solution on resolving the small-scale bed topography.

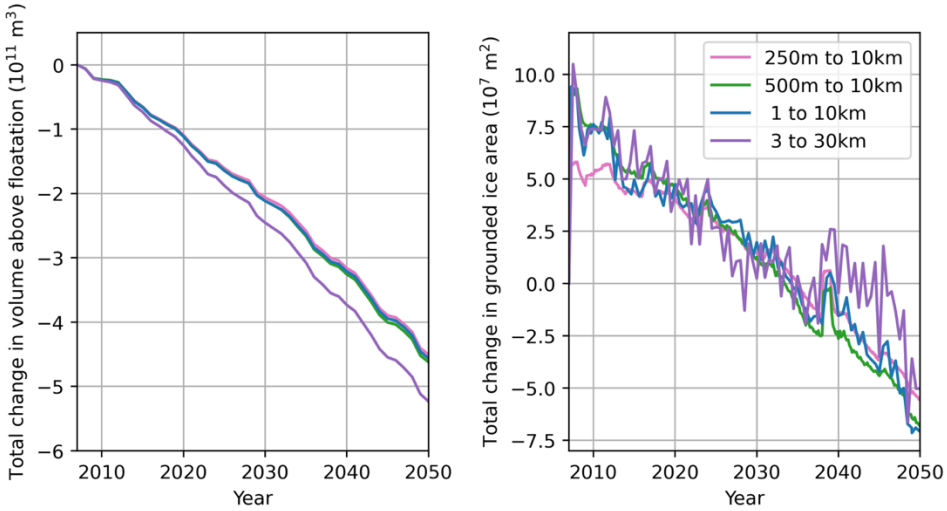

Figure S6: Results of mesh convergence test with smoothed ice thickness and bed topography in terms of change from the initial condition. The 1–10km mesh gives similar results to the 0.5–10 km and 0.25–10 km meshes.

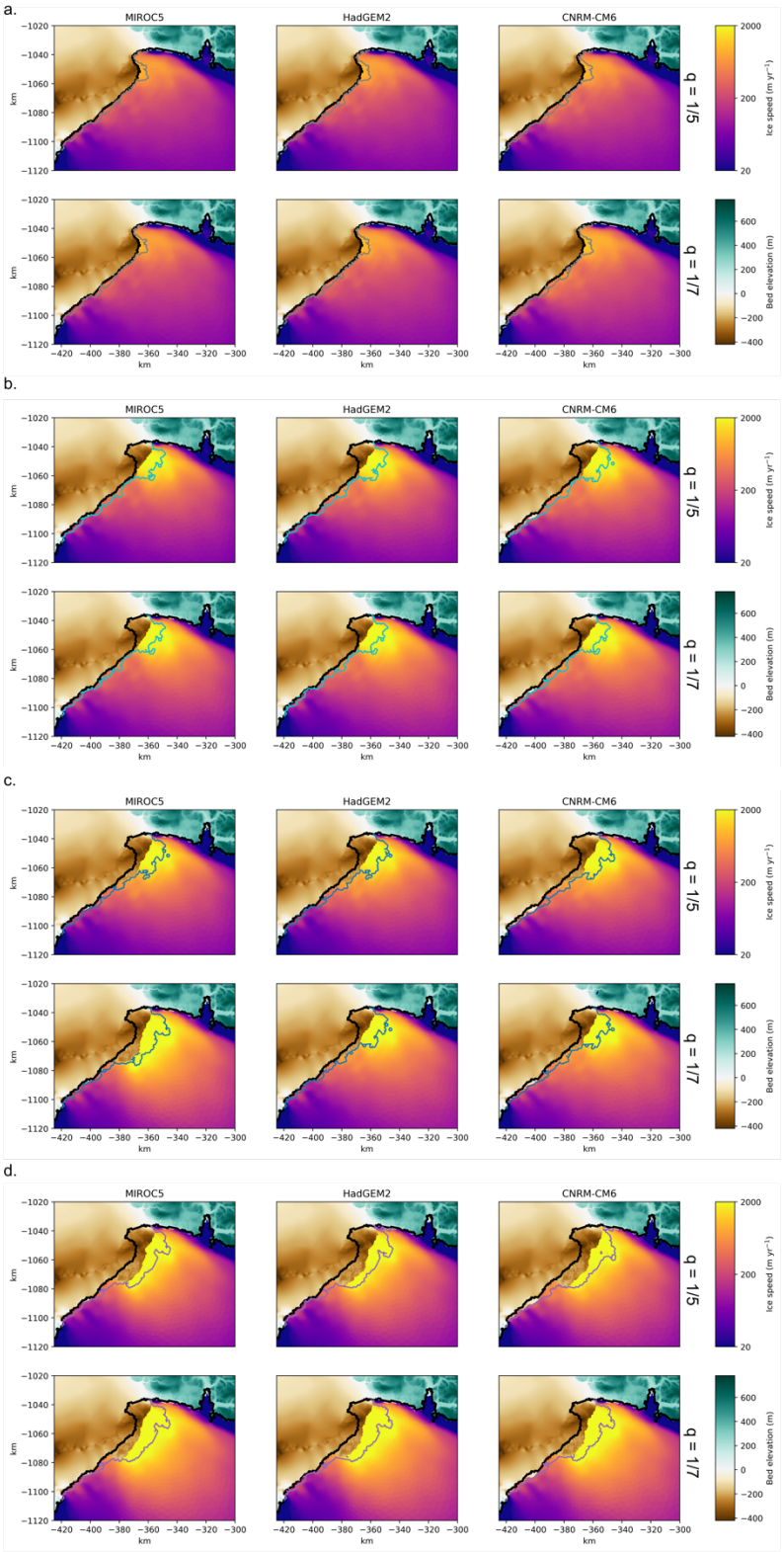

Figure S7: Snapshots of velocity and grounding line position at 2050 for 2017 calving front (a) and von Mises calving runs with high (b), medium (c), and low (d) threshold stresses. Top and bottom rows of each set of subpanels correspond to basal friction law exponents of q=⅕ and q=1/7, respectively. Grounding line colors follow Figure 4 in the main text.

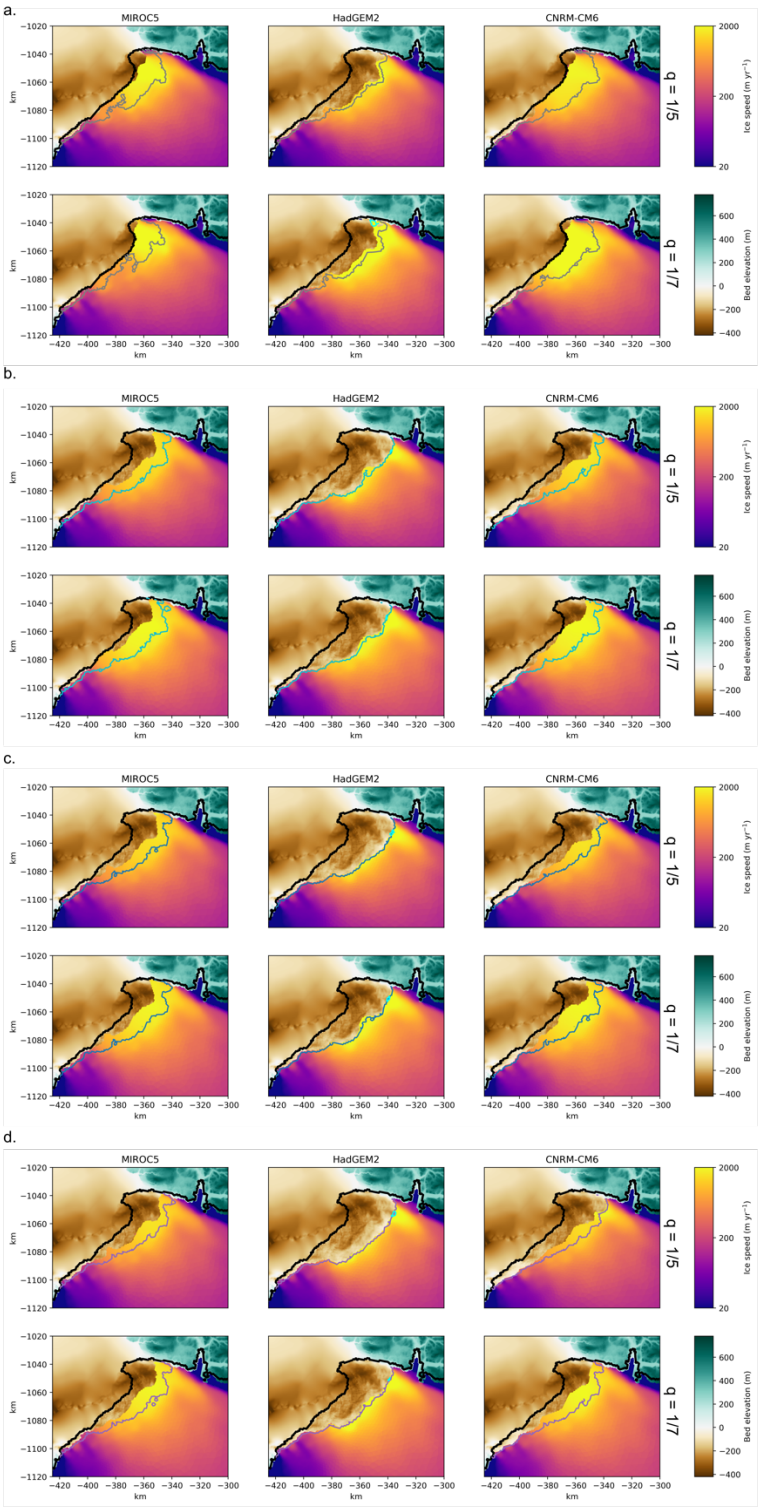

Figure S8: Snapshots of velocity and grounding line position at 2100 for 2017 calving front (a) and von Mises calving runs with high (b), medium (c), and low (d) threshold stresses. The retreat in simulations using the 2017 calving front (a) is due combined surface and sub-marine melting. Top and bottom rows of each set of subpanels correspond to basal friction law exponents of q=⅕ and q=1/7, respectively. Several small areas outlined in light cyan indicate ice flow speeds ≥3 km yr^{-1} (i.e., faster than imposed maximum calving rate). Grounding line colors follow Figure 4 in the main text.

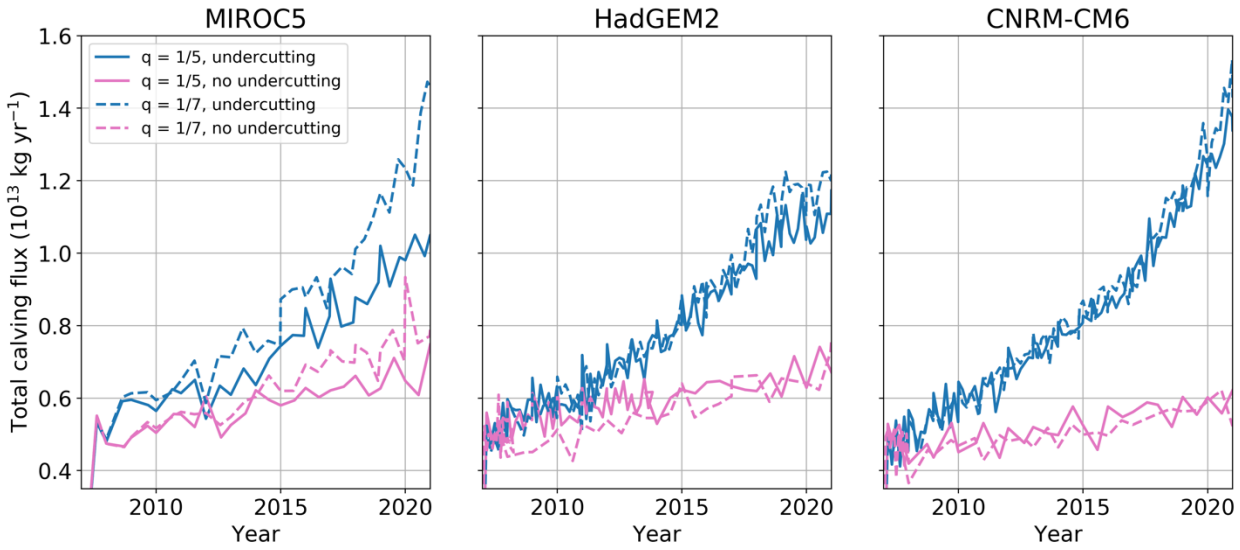

Figure S9: Comparison of simulations from 2007–2021 with undercutting active (blue) and undercutting inactive (pink) for the medium σ_{max} case (see Table 1 in main text). While undercutting is not a large direct contribution to the mass budget (Figure 6 in main text), its control on calving is significant.

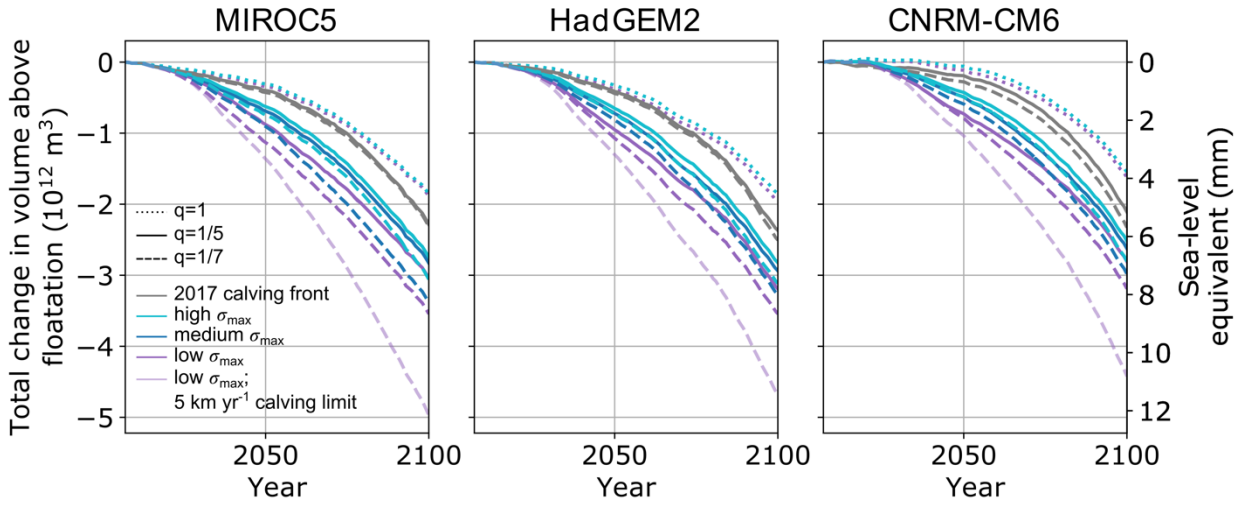

Figure S10: Same as Figure 4 (a–c) in main text, but with upper bound mass loss scenarios (5 km yr^{-1} calving rate limit) included in lavender.